Emulation of a PEM Fuel Cell Stack from its Generic and Polynomial Model using Simulink

LUIS CAMACHO, SECUNDINO MARRERO, CARLOS QUINATOA, CARLOS PACHECO
Department of Electrical Engineering,
University Technical of Cotopaxi,
Barrio El Ejido, Sector San Felipe,
Latacunga,
ECUADOR

Abstract: - This paper will discuss the simulation of a PEMFC fuel cell stack based on its generic characteristics. To achieve the set objective, a fuel cell model capable of replicating its electrical characteristics was developed, showcasing the polynomial approximation-based proposed models and the generic model. The validation of these suggested models involved conducting simulations utilizing converters and comparing the outcomes with those produced by the Simulink fuel cell stack block. The fuel cell instance underwent testing to reproduce the electrical behavior of the cell, devoid of the specific data associated with the fuel cell stack.

Key-Words: - Simulation, Cell, Fuel, Model, Stack, Electrical, Generic, Polynomial, Simulink.

Received: August 29, 2023. Revised: May 2, 2024. Accepted: June 9, 2024. Published: July 26, 2024.

1 Introduction

The growing need for traditional energy sources is imperative for the economic progress of a nation, consequently resulting in the rise of unconventional energy sources utilization like thermal, tidal, wind, solar energy, and fuel cells. These sources are crucial in fulfilling these requirements. Fuel cells, through the utilization of hydrogen and oxygen without combustion, represent a sustainable and eco-friendly energy source, [1].

For the increase in the use of renewable energies, fuel cells represent a prominent option as they produce both heat and energy simultaneously in small installations that are compatible with other sources such as natural gas and photovoltaic systems, [2]. The fuel cell is a device based on electrochemical processes that convert chemical energy into electrical energy. This power source can be utilized in stationary or mobile applications, utilizing hydrogen as its fuel source. It is distinguished by its eco-friendly characteristics, generating water and heat as by-products, [3]. Electricity generation using these devices can be divided into five types: Proton Exchange Membrane Fuel Cells (PEMFC), alkaline fuel cells (AFC), phosphoric acid fuel cells (PAFC), molten carbonate fuel cells (MCFC), and solid oxide fuel cells (SOFC). Their practical application requires pressure stabilizers and the use of controllers for active and reactive power delivery to solve problems related to sudden load changes. For this purpose, converters, filters, and controllers are used, [4]. The implementation of PEMFC-type fuel cells is currently hindered by technical and operational challenges that affect their efficiency and stability. These challenges include the need to develop accurate models considering coupling with dynamic changes, as well as reducing the slow response to changes in electrical load. Additionally, appropriate converter design and consideration of its response to different types of loads are required to comprehensively address these challenges. Optimization of performance demands improvement in the efficiency and adaptability of the cells. Undoubtedly, this contributes to the successful application of sustainable energy systems required today for transitioning towards cleaner energy sources.

The fuel cell demonstrates the capacity to effectively transform the chemical energy of hydrogen into direct current (DC) while avoiding the generation of pollutants. This feature is harnessed in various stationary, portable, and transportation applications. Hydrogen is acquired from an external tank to facilitate its operation. The oxidation of this gas occurs at the anode, whereas the reduction of oxygen from the air takes place at the cathode. This process leads to the production of electricity, water, and heat, [5]. These devices demonstrate a remarkable capacity for adaptation, [6], therefore, they can also be included in a distributed electricity generation network. By

producing energy through a chemical process without the need for direct combustion, they allow for the reduction of carbon dioxide emissions, which are present in the combustion of traditional energy sources. This undoubtedly contributes to greater environmental respect. This is how these latest generation devices such as PEMFC cells achieve efficiencies higher than 50 %, allowing the transformation of chemical energy into electricity, in contrast to the way of operation in conventional batteries, [7]. This allows its ability to mitigate power generation variability, which can be achieved with low inertia power electronic converters to achieve system stability, [8]. This energy source finds a variety of applications, due to the energy efficiency of this technology, especially in PEMFC cells, [9]. In recent decades, our irresponsible lifestyle has led to significant environmental harm, as seen in issues like the depletion of the ozone layer and the phenomenon of global warming, PEMFCs are now recognized as a sustainable alternative, producing water vapor as a by-product, [10]. The interest in power generation through fuel cells, especially those of the PEMFC type, used in small-scale applications, is due to their ability to operate autonomously or connected to the grid, being valuable for generation in remote locations, [11].

Although PEMFC fuel cell power generation devices were initially deployed in aerospace and military applications because of their efficiency , low noise level and environmental friendliness, [12], today have a field of increased employment due to their economic competitiveness and the feasibility of being combined with photovoltaic generation in hybrid systems. They are also found in various applications for the propulsion of automobiles and submarines, [13]. In this situation, the cells have attracted the attention of business investments due to the demand for environmentally friendly power generation as an option to combustion engines for power generation, [14].

Global energy consumption as a general trend is growing every year, and to meet this demand, there has been an increased reliance on renewable sources such as solar and wind energy, which are abundant in certain environments, [15]. However, this technology also faces challenges that restrict its commercial viability, [16]. To perform emulation, a fuel cell model is essential, since the response of the emulator is based on this specific model. In general, fuel cell models tend to be complex or require several tests to obtain the essential parameters for the model to work. The simplicity of the model and ease of obtaining the necessary data for its application are crucial prerequisites, especially in cases where the fuel cell or the appropriate equipment is not available for extensive testing to determine all the fuel cell parameters. For this reason, the present work proposes the study of PEMFC type emulator, by adapting converters to evaluate the behavior of the generic and polynomial model with loads from the data provided by the manufacturer.

2 PEM Type Fuel Cell Model

In the literature, there are several fuel cell models designed to observe how fuel cells behave under specific operating conditions. However, most of these models focus on describing the chemical reactions that take place inside the cell, which makes them complex and specific, making their direct application with electrical components difficult. For this rationale, we move forward with the assessment of various models to select the most suitable one for simulating the behavior of a cell with a simplified structure, as illustrated in Figure 1, which is composed of a membrane and electrode assembly (MEA), which includes an anode and a cathode separated by a PEM. This serves as an electrolyte, aiding in the conduction of protons from the anode to the cathode. In this particular situation, there is a need for a model with the ability to replicate the electrical performance of either a single fuel cell or a group of fuel cells. This model should be developed using the standard data typically included in the specification sheets supplied by the manufacturers of such devices. It is important to note that the majority of manufacturers furnish detailed information regarding these fuel cells, which can be outlined as below:

- I-V curve.
- I-P curve.
- Rated power.
- Operating temperature.
- Nominal hydrogen pressure.
- Hydrogen composition.

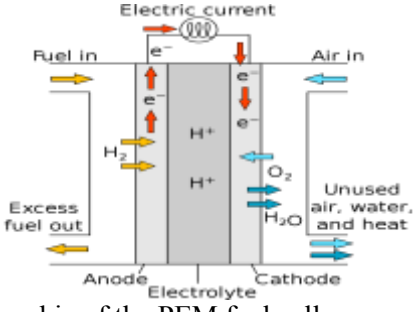

Fig. 1: Graphic of the PEM fuel cell

2.1 Generic PEM Fuel Cell Model

[17], the document introduces a proposal for a universal model of a fuel cell that combines simplicity with comprehensive detail. This model comprises an equivalent circuit consisting of multiple fuel cells functioning under consistent pressure and temperature environments. In order to replicate the system, it is essential to calibrate the voltage levels within the cell at current intensities of 0 A and 1 A, utilizing data derived from the polarization curve supplied by the manufacturer. This data illustrates the fluctuations impacting the open circuit voltage (E_{OC}), the exchange current i_O, and the Tafel slope.

These values can be modified according to equations (1) - (3).

$$E_{OC} = k_c k_n \tag{1}$$

In the context of nominal operating conditions, K_C denotes the constant voltage, while E_N refers to the Nernst voltage, reflecting the thermodynamic voltage of the fuel cell and influenced by factors such as temperature and partial pressure, which are contingent upon the composition of reactants and products within the cell.

The calculation of the exchange current i_O involves the utilization of equation (2).

$$i_O = \frac{zFk(P_H)}{Rh} e^{\frac{\Delta G}{RT}} \tag{2}$$

Additionally, z denotes the quantity of mobile electrons, F corresponds to the Faraday constant which is 96485 As/mol, R stands for the universal gas constant valued at 8.3145 $J/(molK)$, (P_{H_2}) represents the partial pressure of hydrogen within the cell in atmospheres (atm), (P_{O_2}) indicates the partial pressure of oxygen within the cell in atmospheres, k symbolizes the Boltzmann constant, having a magnitude of $1.38\,x\,10^{-23}\,J/K$, h signifies the Planck constant with a value of 6.626 $x\,10^{-34}\,Js$, t, indicates the operational temperature in Kelvin (k), and y $\Delta\,G$ represents the alteration in Gibbs free energy.

$$A = \frac{RT}{\alpha zF} \tag{3}$$

In equation (3), T denotes the operational temperature in Kelvin, while α represents the charge transfer coefficient, which is subject to variation based on the electrode and catalyst type.

The circuit depicted in Figure 2 bears resemblance to the simplified model illustrated in Figure 1. Nevertheless, for the comprehensive model, it is imperative to revise the parameters (E_{OC}),i_O and A.

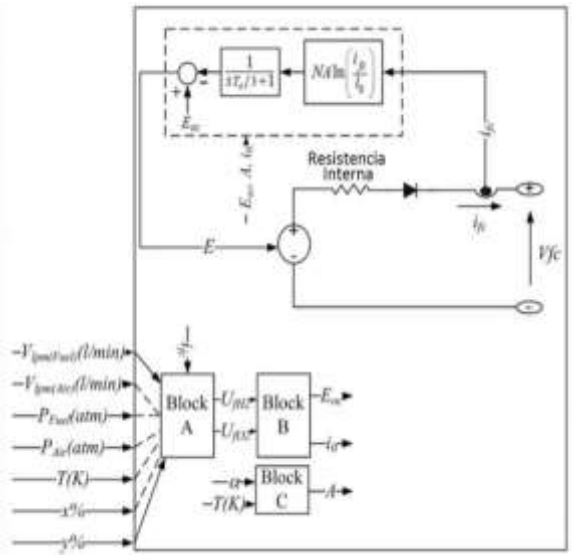

Fig. 2: Equivalent circuit of the stack upon which the detailed model used by Simulink is based

In block A of Figure 2, the conversion efficiency of hydrogen (U_{fH2}) and oxygen (U_{fO2}) is calculated the following expressions:

$$U_{fH_2} = \frac{n_{H_2}^r}{n_{H_2}^{in}} \frac{60000\,RTN_{i_{fc}}}{zFP_{fuel}V_{lpm(fuel)}x\%} \tag{4}$$

$$U_{fO_2} = \frac{n_{O_2}^r}{n_{O_2}^{in}} \frac{60000\,RTN_{i_{fc}}}{zFP_{air}V_{lpm(air)}y\%} \tag{5}$$

P_{fuel} signifies the absolute pressure at which the fuel is provided, while P_{air} denotes the air supply pressure. $V_{lpm(fuel)}$ represents the fuel flow rate in liters per minute (L/min), $V_{lpm(air)}$ indicates the air flow rate in liters per minute (L/min), and x denotes the percentage of hydrogen.

The cell structure shown in Figure 2 represents the equivalent circuit of the stack that would establish the detailed model proposed by [17], where the fuel (%), Y is the percentage of oxygen in the oxidant (%), and the value of 60000 comes from the conversion of the flow rate in liters per minute L/min used by the model into (m^3/s).

Block B calculates the Nernst voltage and the partial pressure of hydrogen, oxygen, and water, through the equations as follows:

$$P_{H_2} = \left(1 - U_{fH_2}\right)x\,\%\,P_{fuel} \tag{6}$$

$$P_{O_2} = \left(1 - U_{fO_2}\right)y\,\%\,P_{air} \tag{7}$$

$$P_{H_2O} = (w + 2y\,\%\,U_{fO_2})P_{air} \tag{8}$$

$$\begin{cases} 1.229 + (T - 298)\frac{-44.43}{zF} + \frac{RT}{zF}\ln\left(P_{H_2}P_{O_2}^{\frac{1}{2}}\right) \\ \qquad when\ T\ \leq 100^{\circ} \\ 1.229 + (T - 298)\frac{-44.43}{zF} + \frac{RT}{zF}\ln\left(\frac{P_{H_2}\,P_{O_2}^{\frac{1}{2}}}{P_{H_2O}}\right) \\ \qquad when\ T\ > 100^{\circ} \end{cases} \quad (9)$$

In equation (8), P_{H_2O} represents the partial pressure of water vapor within the stack, while w signifies the proportion of water vapor in the oxidant (%). The revised values for the open circuit voltage (E_{OC}) and the exchange current (i_O) can be determined based on the partial pressures of the gases and the Nernst current.

Block C is tasked with computing the updated values for the Tafel slope. The parameters α, ΔG, and K_c are derived from the polarization curve during standard operating conditions. To determine the maximum voltage values (U_{fH}) and (U_{fO}), equations (10) and (11) are used respectively.

$$U_{fH_2} = \frac{\eta_{nom}\Delta h^0(H_2O(gas))N}{zFV_{nom}} \quad (10)$$

$$U_{fO_2} = \frac{60000\ RT_{nom}NI_{nom}}{0.42\ zFP_{air_{nom}}V_{lpm(air)nom}} \quad (11)$$

Where η nom represents the nominal efficiency of the stack (%), with the nominal heating value; $\Delta h^0(H_2O)$(gas)) is a constant equal to $241.83\ x\ 103\ J/mol$; V_{nom} is the nominal voltage, I_{nom} is the nominal current, $V_{lpm(air)_{nom}}$ is the nominal air flow rate (L/min); $P_{air_{nom}}$ is the nominal absolute pressure of air supply in Pascales (Pa) y T_{nom} is the nominal operating temperature. From these conversion rates, the nominal partial pressures of the gases and the Nernst voltage can be calculated.

By considering the values of E_{OC}, i_O, and A, along with the assumption of the stack operating at constant conversion rates or under nominal conditions, it is possible to ascertain the parameters α, ΔG, and K_c. In cases where fuel or air are unavailable at the input terminals of the cell, the fuel cell stack module is engineered to function at a constant gas conversion rate (referred to as nominal conversion rate). This involves modifying the gas intake in order to provide a slightly excess amount than required across all loads.

The peak maximum voltage ($U_{fO_{2(peak)}}$) and its corresponding voltage variation (V_u) are employed to illustrate the influence of oxygen depletion (resulting from the delay in the air compressor) on the cell voltage (E_n) produced by the cell, as determined by equation (12):

$$E_n = \begin{cases} E_n - k\left(U_{fO_2} - U_{fO_{2(peak)}}\right) & U_{fO_2} > U_{fO_{2(nom)}} \\ E_n & U_{fO_2} > U_{fO_{2(nom)}} \end{cases} \quad (12)$$

Where ($U_{fO_{2(pico)}}$) represents the nominal oxygen usage, and K is the constant associated with the voltage undershoot, which is determined in equation (13):

$$K = \frac{V_u}{K_c(U_{fO_{2(peak)}}U_{fO_{2(nom)}})} \quad (13)$$

2.2 Fuel Cell Emulator

In the academic literature, numerous fuel cell emulation systems have been documented. These systems typically rely on DC-DC converters, as outlined in study, which utilizes a Buck converter, and in where emulation for an electric vehicle is carried out. The control of these emulators is commonly overseen by FPGAs, necessitating the customization of the fuel cell model to suit the specific device under consideration. When employing a DC-DC converter, the intricacy of the emulation system escalates, as it involves not only modeling the fuel cell but also designing the converter and taking into account its electrical response. In this context, our focus will be directed towards analyzing in depth the emulation system put forth in the academic literature.

2.2.1 FPGA-based Fuel Cell Emulation

Various systems have been documented in the literature to replicate the functionality of the fuel cell, [18], proposing a simulation system that leverages an FPGA as its foundation. The authors delineate in their research the architecture of a fuel cell model in VHDL, aiming to integrate it into an FPGA. This approach utilizes bipolar transistors and passive elements to depict the power condition of the fuel cell.

Figure 3 illustrates the overall diagram of the emulator, emphasizing the flow of digitized current input to the controller, which in turn produces the digitized output voltage. In order to accomplish this, a 10-bit resolution analog-to-digital converter is utilized with a full-scale voltage range of 2V in the generation of the current waveform, converting it into a bit stream that reflects the visualized current signal, [18].

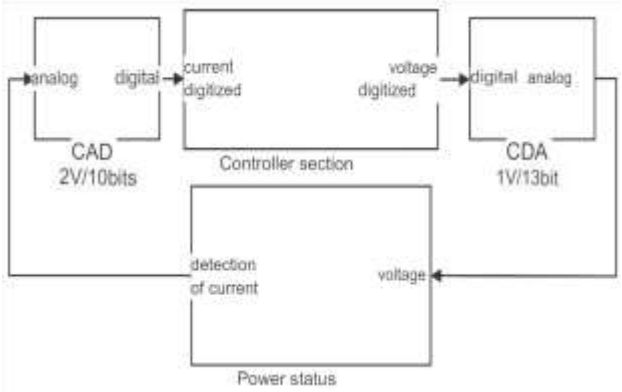

Fig. 3: Block diagram of the FPGA-based emulator

Following this, the voltage that has been digitized is transformed into analog form by utilizing a digital-to-analog converter possessing a 1V full-scale voltage range and 13 bits, while adjusting the gain of the conversion process with the help of an operational amplifier. Furthermore, both pnp and npn transistors are employed as emitter followers to ensure a voltage gain of unity and to prevent any direct current offset by linking an npn transistor with a pnp BJT, as depicted in Figure 4, [18].

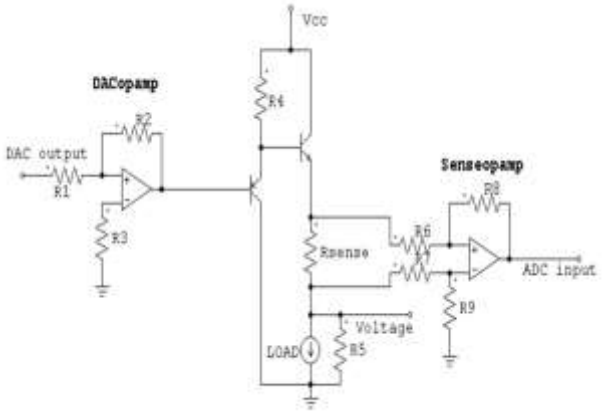

Fig. 4: Gain stage for FPGA-based emulation system

The model utilized in this study is segmented into two components: a dynamic segment and a steady-state segment. The steady-state portion illustrates the I-V characteristic curve of the fuel cell system over the complete temperature spectrum. An average value is computed based on a group of standard features at 30°C, which is subsequently fine-tuned utilizing a specific equation.

Equation (14) is employed to ascertain the voltage value (VFC) across the cell.

$$V_{FC} = A - B_{ln}\left(1\frac{I_{FC}}{C}\right) - D\ e^{\frac{i_{FC}}{E}} \qquad (14)$$

IFC denotes the electric current flowing through the fuel cell, while VFC indicates the electric potential difference across the cell. A collection of isothermal I-V curves has been produced for every particular temperature.

Equation (15) can be utilized to articulate the output voltage of the steady-state model.

$$V(i,T) = V_{mod}\left(i, 30^{\circ}C\right) + C(i,T) \qquad (15)$$

The output voltage at a temperature T, under a specific current of the fuel cell i is denoted by $V(i,T)$. The output of the steadystate isothermal model for the same current i but at a reference temperature of 30°C is represented by $Vmod\ (i,$ 30°C). The output in the correction subsystem, denoted by $c(i,T)$, reflects a temperature T different from the nominal temperature of 30°C through equation 16.

$$C(i,T1) = C_0(T_1)i^{\circ} + C(T_1)i + C_0(T_2)i^2 + C_3(T_1)i^3 \qquad (16)$$

The FPGA emulation system's dynamic component is linked in parallel with the stable section. The model's output corresponds to the dynamic part's input, generating a specific current. This current is combined with the external current to create the steady-state current signal, utilized as the stable section's input. Utilizing frequency response analysis (FRA), the dynamic model is defined. The impedance transfer function is assessed within the appropriate frequency range of 0 to 200 kHz. To strike a balance between model complexity and accuracy, three poles and three zeros are chosen.

The dynamic component is realized through the utilization of a digital filter that replicates the transfer function within the z-domain, as specified in equation (17), derived through the application of the Euler transform to the estimated transfer function.

$$Fz = a_0 + \frac{a_1}{z-b_1} + \frac{a_2}{z-b_2} + \frac{a_3}{z-b_3} \qquad (17)$$

2.3 Polynomial Approximation Model

The fuel cell model using polynomial approximation is derived from the fuel cell stack block in Simulink/Matlab. This block is essential for obtaining the individual points of the I-V curve of the stack intended to be modeled through this approach. Knowledge of certain fuel cell data is required to use this block, which necessitates information on the following parameters:

- Voltage at 0 A.
- Voltage at 1 A.
- Current at Nominal Operating Point (PON).
- Voltage at PON.
- Current at Maximum Operating Point (POM).
- Voltage at POM.
- Number of cells.
- Nominal stack efficiency.
- Operating temperature.
- Nominal air flow rate.
- Nominal hydrogen pressure H_2.
- Nominal air pressure.
- Nominal hydrogen composition H_2.
- Nominal air composition.

The mentioned information can be extracted from the manufacturer's technical documentation. Some of these details are presented explicitly, while data such as voltage at different current values, the current at the turn on state PON, the voltage at PON, the current at the POM, and the voltage at POM are derived from the typically provided I-V and I-P curves by the manufacturer. To find the PON, it is essential to consider both the I-V and I-P curves, where the PON will be identified as the point of intersection between both curves. Once this point is located, the voltage and current values on the I-V curve at that point are examined, being these values (V_{PON}) and the current (I_{PON}), respectively. To determine the POM, the maximum power level (P_{max}) on the I-P curve must be located, and the corresponding current at that point is observed; this value will be the current (I_{POM}). Then, the voltage associated with (I_{POM}) on the I-V curve is verified, and this is the voltage (V_{PON}). This graph with the aforementioned points can be observed in Figure 5.

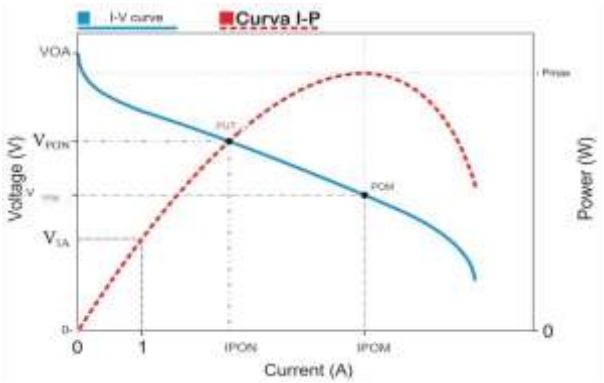

Fig. 5: Processing of voltage at 0 and 1 A, current and voltage at PON and current and voltage at POM

Once all the essential data has been gathered, the simulation of the fuel cell stack can be executed in Simulink/Matlab.

3 Development of the Fuel Cell Emulation System

To ensure proper operation and attainment of the required characteristics for a fuel cell in a specific application, it is essential to have a deep understanding of its performance under operating conditions. Fuel cells can exhibit high sensitivity to various factors such as changes in reactant pressure, temperature fluctuations, humidity levels, reactant concentration and purity, as well as variations in applied load. Therefore, accurate prediction of the fuel cell's response to these stimuli is of utmost importance. While there are numerous studies on fuel cell emulation in the literature, most require conducting tests and characterizing the actual cell to replicate its performance. Consequently, this study has developed a straightforward approach to emulate the cell, eliminating the need to rely on it or decipher a complex model. To analyze the performance of the fuel cell and evaluate the polynomial model, simulations were conducted using the gathered information to verify the response of the proposed model.

3.1 Simulation of a Fuel Cell with the Fuel Block Cell Stack

In order to establish a complete connection with the fuel cell stack block in Simulink/MATLAB, which is based on the detailed model in section 2.1 and considering that at that time a specific type of fuel cell stack was not available to extract the necessary parameters, it was decided to use the fuel cell stacks defined by [17]. Therefore, the simulation scheme obtained can be observed in Figure 6, which includes three sets of PEM fuel cell stacks with capacities of 1.26 kW, 6 kW and 50 kW. In this situation, the 6 kW fuel cell stack was used, whose parameters are detailed in Table 1.

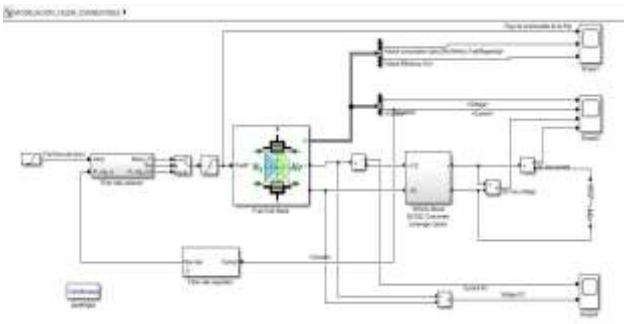

Fig. 6: Simulation diagram in Simulink

To carry out the simulation, other subsystems are necessary to observe the behavior of the cell. Consequently, a gas supply system and a boost converter with an RL load adjusted to a constant

voltage of 100V were implemented, as shown in Figure 7 and Figure 8.

The proposed block in Simulink is already equipped with outputs that enable the observation of various cell parameters, such as efficiency, gas consumption, flow rate, composition, Tafel curve slope, exchange current, Nernst voltage and open circuit voltage.

Table 1. Parameters of the 6 kw fuel cell stack

Fuel Cell Stack Parameters	
Battery power rating	5998.5 W
Maximum battery power	8325 W
Fuel cell resistance	0.07833
Single cell Nerst voltage (E_n)	1.1288 V
Nominal use of H_2	99.56 %
Nominal utilization (O_2)	59.3 %
Nominal fuel consumption	60.38 SLPM
Nominal air consumption	143.7 SLPM
Exchange current (i_O)	0.29197
Exchange ratio (α)	0.60645
Fuel composition x_{H_2}	99.95 %
Oxidant composition y_{H_2}	21 %
Ratio of nominal fuel flow to utilization H_2 nominal	50.06 LPM
Maximum fuel flow ratio at nominal utilization (H_2)	84.5 LPM
Maximum air flow ratio at nominal utilization of (O_2)	506.4 LPM
System temperature (T)	338 K
Fuel feed pressure (P_{Fuel})	1.5 bar
Air supply pressure (P_{Fair})	1 bar

3.1.1 Generic Fuel Cell Simulation Results

During the simulation, the behavior of the fuel cell stack while operating under the power demand imposed by the Boost converter was monitored. Examination was conducted on the voltage and current levels at both the fuel cell output and the RL load of the converter.

Within Figure 7, the gas flow rate provided was also observed, alongside the consumption of hydrogen and oxygen by the fuel cell. It was observed that the fuel flow rate stabilized at 50 lpm and remained consistent for a duration of 10 seconds before initiating a linear increase.

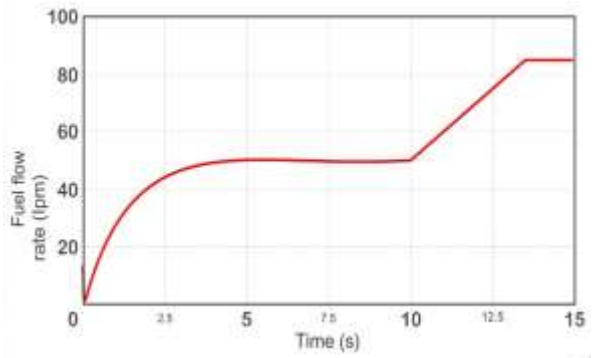

Fig. 7: Graph of the fuel flow rate of the stack

This phenomenon is explained by observing that by providing more fuel than the stack consumes (Figure 8), waste occurs, resulting in lower efficiency.

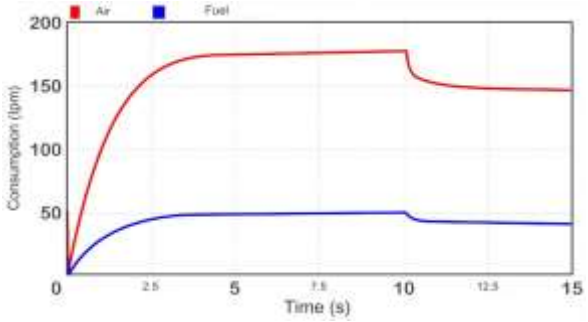

Fig. 8: Graph of the reactant consumption of the stack

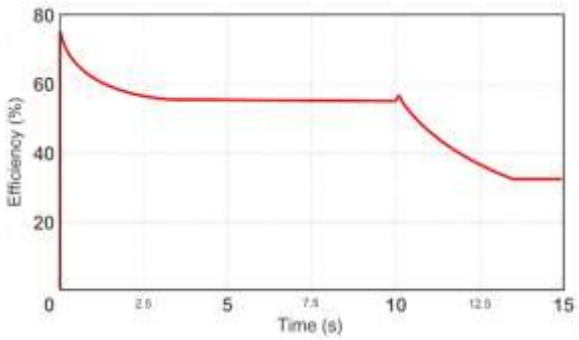

Fig. 9: Graph of the stack efficiency

The rise in the flow rate led to a reduction in the stack efficiency as depicted in Figure 9.

Furthermore, the behavior shown in Figure 9 of the stack efficiency leading to a decrease in voltage and an increase in current is reflected in Figure 10 and Figure 11.

Then, around 3.5 seconds, the flow rate at the cell inlet becomes constant again, and the other parameters stabilize.

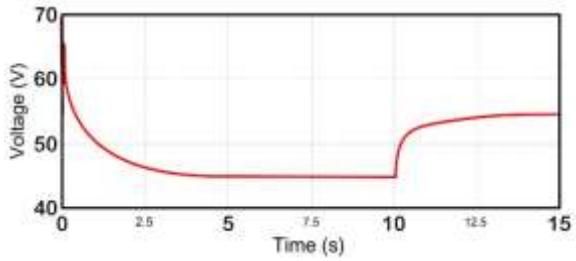

Fig. 10: Graph of stack voltage

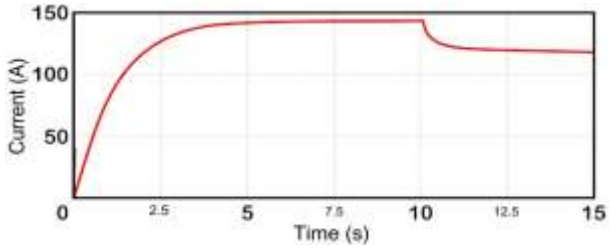

Fig. 11: Graph of stack current

3.2 Simulation of 20 W Fuel Cell Stack

The objective of this simulation was to assess the performance of a fuel cell and derive its I-V characteristic using a polynomial estimation. A 20 W system was chosen, and its specifics are outlined in Table 2. These specifics, in conjunction with the current, voltage, and power characteristics, equip us with the essential parameters for the simulation, all sourced from the specification document provided by fuel cell store, the vendor of this unit. Key parameters needed for the simulation encompass the voltage and current at the designated PON and POM, which were established as described in section (2.3) of the polynomial estimation model for a power output of 20 W.

Table 2. Parameters of the 20 Kw fuel cell stack

Parameter	Value
Number of cells	10
Power	20 W
Performance	6 V @ 3.4 V
Reactives	Hydrogen and Air
Operating temperature	$60^{\circ}C$
Pressure of the $\boldsymbol{H_2}$	0.45 – 0.55 Bar
Purity of $\boldsymbol{H_2}$	≥ 99.995
Flow ratio at maximum output	0.25 Lpm
Efficiency	40 % full power

The data obtained from Table 2, along with the graphical depiction of the I-V curve, provide all the necessary components for developing a thorough portrayal of the fuel cell stack and conducting the simulation. The detailed data is outlined in Table 3.

Table 3. Data required for the 20 W fuel cell stack simulation

Parameter	Value
Voltage a 0 A	9.6 V
Voltage a 1 A	7.35 V
Current in PON	2.5 A
Voltage in PON	6.1 V
Current in POM	4 A
Voltage in POM	5 V
Number of cells	10
Nominal stack efficiency	40 %
Operating temperature	$60^{\circ}C$
Nominal airflow ratio	0.25 Lpm
Nominal pressure $\boldsymbol{H_2}$	0.50 bar
Nominal air pressure	2.5 bar
Nominal composition of the $\boldsymbol{H_2}$	99.995 %
Nominal air composition	Oxygen 21 % Humidity 0.5 %

Once the essential data had been gathered for configuring the fuel cell stack block in Simulink/Matlab, which represents the fuel cell stack, it was linked to a DC-DC converter responsible for maintaining a consistent voltage of 9.6 V on the load side. This enabled the execution of a current scan to encompass all the polarization regions of the 20 W fuel cell stack, as depicted in Figure 12. In contrast to the initial simulation (Figure 6), the utilization of a flow selection block was omitted on this occasion. The rationale behind this decision lies in the primary objective of merely observing the stack's performance under optimal circumstances. In the absence of a block facilitating fuel and/or air input to the stack, it is presumed that the stack functions at a consistent gas conversion rate. This implies that the gas provision is regulated in alignment with the current to guarantee a slightly excessive supply to the stack, irrespective of the load.

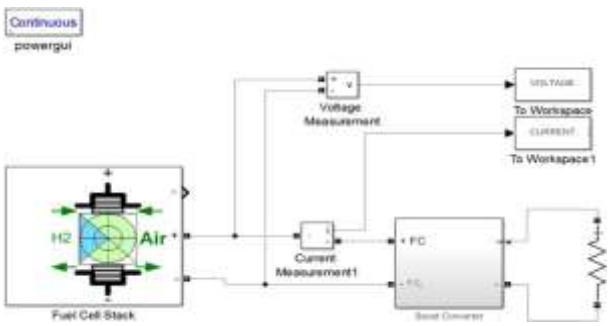

Fig. 12: 20 W Fuel cell stack simulation diagram

During the simulation development, voltage and current measurements were taken and these data were recorded and subsequently used to construct a

graphical representation of the relationship between voltage and current. This allowed us to generate the characteristic curve of the fuel cell, as seen in Figure 13.

Understanding this curve is crucial for comprehending the behavior and performance of the cell under various operating conditions, as described in the simulation results section for a specific stack.

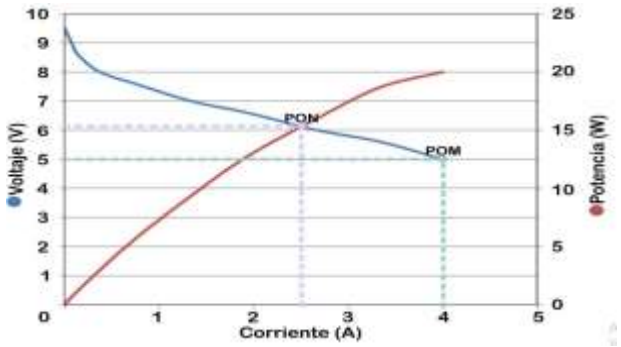

Fig. 13: I-V and I-P plots of the 20 W fuel cell are presented

3.2.1 Simulation Results of a Specific Stack

In the simulation of the 20W stack, the Boost converter was adjusted to provide a constant output of 11.5 V to the load resistive, aiming to characterize the stack and obtain its I-V curve, as illustrated in Figure 14. Here, it is demonstrated how the voltage at load resistive remains around 11.5 V with very little variation.

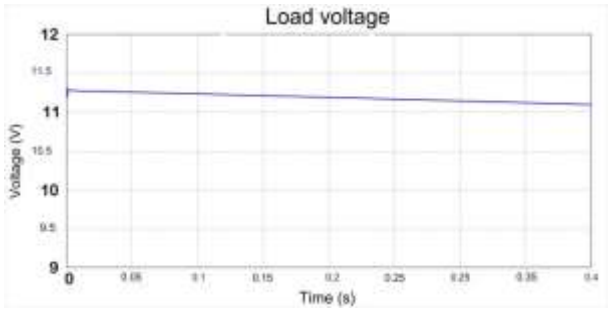

Fig. 14: Load voltage graph

Figure 15 provides a detailed visual representation of how the voltage in the cells evolves over time. It is clearly observed that the initial voltage, recorded at 10.5 V, coincides with the maximum level reached under open circuit conditions, where the current is zero, marking the starting point before the load connection is established. Upon activation of the load, there is a rapid decrease in voltage, dropping to 5.5 V, and this steep decline indicates the transition of the fuel cell to a state where it begins to supply current to the external load. As the load demands more current, the voltage continues to gradually decrease, reaching a value of 5.3 V. The gradual decrease in voltage is indicative of the impact caused by the rising current requirements, leading to a progressive reduction in the voltage of the fuel cell.

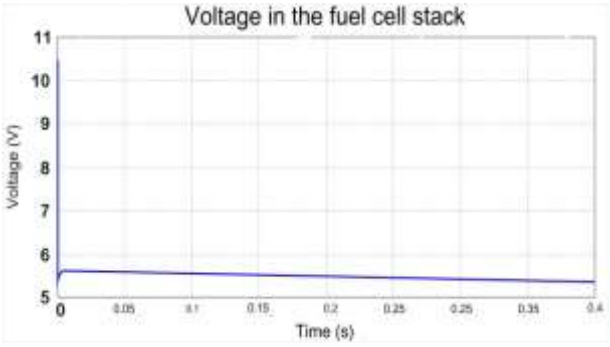

Fig. 15: Fuel cell stack voltage plot

Figure 16 illustrates the dynamics of the current in the stack, which starts at zero when the load is disconnected and increases abruptly to 3.2 A as soon as the converter starts operating. It then gradually increases as the load adjusts the output voltage to keep it constant.

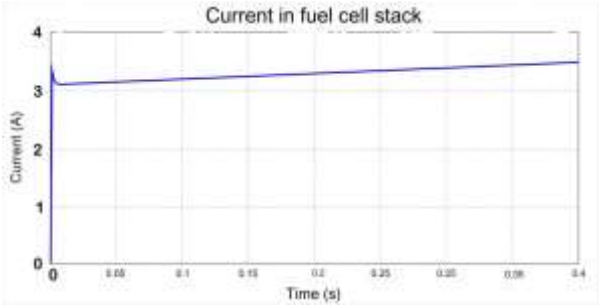

Fig. 16: Fuel cell stack current plot

Figure 17 provides a detailed graphical representation of the current-voltage (I-V) curve corresponding to the 20 W fuel cell. This curve is essential for understanding the electrical behavior under different operating conditions. By analyzing this curve, three distinct polarization regions can be clearly identified, each associated with different loss mechanisms. The first polarization region is related to activation loss, where a significant voltage drop is observed as the current increases. This loss is associated with the energy required to initiate and sustain electrochemical reactions in the fuel cell. The second polarization region is linked to ohmic loss, characterized by a constant and linear decrease in voltage as the current increases. Finally, the third region is associated with mass transfer loss, where the voltage continues to decrease as the current increases, but at a slower rate than in the previous regions.

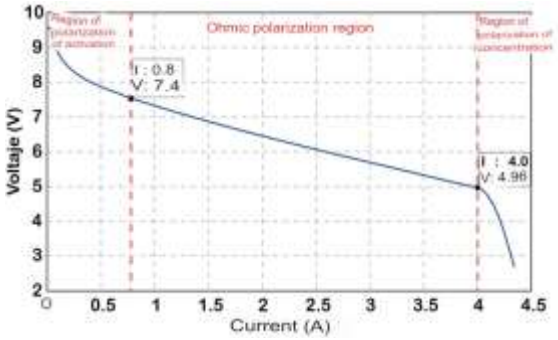

Fig. 17: 20 W fuel cell I-V curve

Additionally, the cell efficiency, estimated at approximately 37.5%, is visualized in Figure 18.

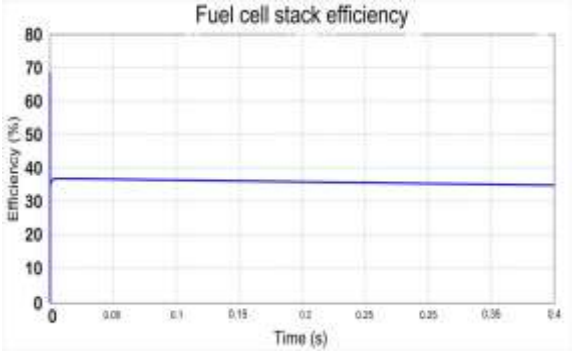

Fig. 18: 20 W fuel cell stack efficiency chart

This efficiency value is crucial for assessing the overall performance of the stack and provides valuable information for future improvements in fuel cell system design and optimization, [19].

4 Conclusion

In this work, a fuel cell emulator has been developed, serving as a valuable tool for fuel cell evaluation. This emulator allows for testing without the need for large laboratory investments when evaluating cell behavior in specific applications, thereby avoiding risks of damage when subjecting it to extreme operating points. Experimental results indicate that the emulator satisfactorily reproduces the cell's electrical behavior in response to load and temperature variations. To simulate the fuel cell model using polynomial approximation, the necessary parameters can be obtained through tests applied to the cell stack to be emulated. The generic fuel cell model combines electrical and electrochemical characteristics, being usable from general data of the fuel cell stack.

According to the model developed in this work, it is concluded that it is possible to generate the cell's electrical behavior without having all its data, and simulation results suggest that the models proposed in this work are suitable, as the responses obtained are very similar to those achieved using the Simulink fuel cell stack block. However, when the fuel cell or the appropriate instruments for testing are not available, nor are all the specific details of the cell in question, the direct application of the mentioned models becomes unfeasible. In such circumstances, the lack of access to the cell and necessary data hinders the effective implementation of the previously described models.

Acknowledgement:
The student author, Luis Camacho, would like to acknowledge and thank the research professors Secundino Marrero and Carlos Quinatoa for their advice, guidance, and knowledge throughout his studies. Also to Professor Carlos Pacheco for his guidance. Thank you very much.

Declaration of Generative AI and AI-assisted Technologies in the Writing Process

During the preparation of this work the authors used typeset.io in order to improve the wording. After using this tool/service, the authors reviewed and edited the content as needed and takes full responsibility for the content of the publication.

References:

[1] A. Koushal, A. Singh, H. R. Anand, Y. K. Chauhan, and R. K. Pachauri, "Modelling and Analysis of Adaptive Fuzzy Controller for the Fuel Cell System," in *2018 International Conference on Power Energy, Environment and Intelligent Control, PEEIC 2018*, Greater Noida, India: Institute of Electrical and Electronics Engineers Inc., Jul. 2018, pp. 208–215. doi: 10.1109/PEEIC.2018.8665574.

[2] V. Boscaino, R. Miceli, G. Capponi, and D. Casadei, "Fuel cell modelling and test: Experimental validation of model accuracy," in *International Conference on Power Engineering, Energy and Electrical Drives*, Istanbul, Turkey, 2013, pp. 1795–1800. doi: 10.1109/POWERENG.2013.6635890.

[3] A. Soltanieh and O. Ogun, "Identification of Nonlinear Multi Input Multi Output Model of PEM Fuel Cell Stack System," in *26th Iranian Conference on Electrical Engineering, ICEE 2018*, Mashhad, Iran: Institute of Electrical and Electronics Engineers Inc., Sep. 2018, pp. 887–892. doi:

10.1109/ICEE.2018.8472595.

[4] B. Banyat, "Modeling and Analysis of Fuel Cell Systems for Stationary Applications," in *2020 International Conference on Power, Energy and Innovations (ICPEI)*, Chiangmai, Thailand: IEEE, 2020, pp. 129–132. doi: 10.1109/ICPEI49860.2020.9431570.

[5] A. Taieb, S. Mukhopadhyay, and A. Al-Othman, "Dynamic Model of a Proton-Exchange Membrane Fuel Cell using Equivalent Electrical Circuit," in *2019 Advances in Science and Engineering Technology International Conferences (ASET)*, Dubai, United Arab Emirates: Institute of Electrical and Electronics Engineers Inc., 2019, pp. 1–4. doi: 10.1109/ICASET.2019.8714573.

[6] P. V Belyaev, V. S. Mischenko, D. A. Podberezkin, and R. A. Em, "Simulation modeling of proton exchange membrane fuel cells," in *2016 Dynamics of Systems, Mechanisms and Machines (Dynamics)*, Omsk, Russia, 2016, pp. 1–5. doi: 10.1109/Dynamics.2016.7818980.

[7] Z. Huang, J. Zhou, and Y. Cui, "Performance Simulation of Proton Exchange Membrane Fuel Cell System Based on Fuzzy Logic," in *2020 IEEE Conference on Telecommunications, Optics and Computer Science, TOCS 2020*, Shenyang, China: Institute of Electrical and Electronics Engineers Inc., Dec. 2020, pp. 382–384. doi: 10.1109/TOCS50858.2020.9339730.

[8] J. Khazaei, F. Moazeni, B. Trussell, and A. Asrari, "Small-signal Modeling and Analysis of a Grid-Connected PEM Fuel Cell," in *51st North American Power Symposium, NAPS 2019*, Wichita, KS, USA: Institute of Electrical and Electronics Engineers Inc., Oct. 2019, pp. 1–6. doi: 10.1109/NAPS46351.2019.9000355.

[9] M. M. Barzegari, E. Alizadeh, M. Khorshidian, S. M. Rahgoshay, and S. H. M. Saadat, "Nonlinear Grey-Box Modeling and Model Predictive Control for Cascade-Type PEM Fuel Cell Stack," in *2017 IEEE Vehicle Power and Propulsion Conference, VPPC 2017 - Proceedings*, Belfort, France: Institute of Electrical and Electronics Engineers Inc., Apr. 2018, pp. 1–5. doi: 10.1109/VPPC.2017.8330979.

[10] R. I. Salim, "The performance of ACO in the parameter identification of a pem fuel cell model in comparison to GA and PSO," in *5th International Conference on Power Generation Systems and Renewable Energy Technologies, PGSRET 2019*, Istanbul, Turkey: Institute of Electrical and Electronics Engineers Inc., Aug. 2019, pp. 1–6. doi: 10.1109/PGSRET.2019.8882690.

[11] H. S. Das, C. W. Tan, A. H. M. Yatim, and N. D. Bin Muhamad, "Modeling and simulation of stand-alone fuel cell system for distributed generation application," in *2016 3rd International Conference on Electrical Engineering and Information and Communication Technology, iCEEiCT 2016*, Dhaka, Bangladesh: Institute of Electrical and Electronics Engineers Inc., Mar. 2017, pp. 1–6. doi: 10.1109/CEEICT.2016.7873043.

[12] Z. Ren, Y. Huangfu, R. Xie, and R. Ma, "Modeling of Proton Exchange Membrane Fuel Cell Based on LSTM Neural Network," in *Proceedings - 2020 Chinese Automation Congress, CAC 2020*, Shanghai, China: Institute of Electrical and Electronics Engineers Inc., Nov. 2020, pp. 7314–7317. doi: 10.1109/CAC51589.2020.9326514.

[13] A. S. Kumar, T. Cermak, S. Misak, and B. Horak, "Modeling and simulation for 1.2 kW PEM fuel cell power generation of isolated load conditions," in *2015 International Conference on Electrical Drives and Power Electronics, EDPE 2015 - Proceedings*, Tatranska Lomnica, Slovakia: Institute of Electrical and Electronics Engineers Inc., Nov. 2015, pp. 235–240. doi: 10.1109/EDPE.2015.7325299.

[14] S. V. M. Guaitolini, I. Yahyaoui, J. F. Fardin, L. F. Encarnacao, and F. Tadeo, "A review of fuel cell and energy cogeneration technologies," in *2018 9th International Renewable Energy Congress, IREC 2018*, Hammamet, Tunisia: Institute of Electrical and Electronics Engineers Inc., May 2018, pp. 1–6. doi: 10.1109/IREC.2018.8362573.

[15] N. Shamim, A. Bilbao, D. Reale, and S. Bayne, "Analysis of grid connected fuel cell power system integrated with supercapacitor," in *IEEE Green Technologies Conference*, Austin, TX, USA: IEEE Computer Society, Jun. 2018, pp. 61–64. doi: 10.1109/GreenTech.2018.00020.

[16] M. S. Ben Yahia, W. Andari, H. Allagui, and A. Mami, "Nonlinear modeling impedance electrochemical of PEM fuel cell," in *2017 18th International Conference on Sciences and Techniques of Automatic Control and*

Computer Engineering, STA 2017 - Proceedings, Monastir, Tunisia: Institute of Electrical and Electronics Engineers Inc., Mar. 2018, pp. 334–337. doi: 10.1109/STA.2017.8314840.

[17] N. M. Souleman, O. Tremblay, and L. A. Dessaint, "A generic fuel cell model for the simulation of fuel cell vehicles," in *5th IEEE Vehicle Power and Propulsion Conference, VPPC '09*, Dearborn, MI, USA, 2009, pp. 1722–1729. doi: 10.1109/VPPC.2009.5289692.

[18] V. Boscaino, G. Capponi, and F. Marino, "FPGA implementation of a fuel cell emulator," in *SPEEDAM 2010 - International Symposium on Power Electronics, Electrical Drives, Automation and Motion*, Pisa, Italy, 2010, pp. 1297–1301. doi: 10.1109/SPEEDAM.2010.5542090.

[19] B. R. Naidu, G. Panda, and R. Ganesh, "Modelling and Hardware-in-Loop validation of a modified controller for intermittent operation of a standalone low voltage DC fuel cell system," in *IEEE Region 10 Annual International Conference, Proceedings/TENCON*, Singapore: Institute of Electrical and Electronics Engineers Inc., Feb. 2017, pp. 1429–1434. doi: 10.1109/TENCON.2016.7848251.

Contribution of Individual Authors to the Creation of a Scientific Article (Ghostwriting Policy)

- Luis Camacho is responsible for identifying research topics, collecting system data, design and implemen- tation, simulation, original drafting and revisions.
- Secundino Marrero and Carlos Quinatoa are dedicated to improving the research topics and scope, working on the methodology, providing technical advice, refining the simulation scenarios, reviewing the results, formatting and editing the final draft, as well as reviewing the revised article to ensure that it meets the publisher's requirements.
- Carlos Pacheco is responsible for revising the text and improving the translation of the article.

Sources of Funding for Research Presented in a Scientific Article or Scientific Article Itself

No funding was received for conducting this study.

Conflict of Interest

The authors state that they have no financial interests or personal relationships that could affect the work done in this study.